From Mixing-Demixing to Condensation-Evaporation Phase Transition in Binary Liquids

Bruno D'Aguanno and Carlo Nardone
CRS4
Centro di Ricerca, Sviluppo e Studi Superiori in Sardegna,
Via N. Sauro, 10, I - 09123 Cagliari

Binary fluid mixtures show first order phase transition phenomena which are either classified as mixing-demixing (phase separation), or as condensation-evaporation. The localization of the transition lines, the characterization of the new phases, and the analysis of the parameters which force model systems to choose one of the two transition mechanisms is the aim of this study. We performed both Parallel Molecular Dynamics simulations and integral equation theory calculations on binary mixtures of Lennard-Jones particles. By fixing the composition and by varying the interaction strength, we found a continuous change between the two kind of transition mechanisms. Theoretical and simulation results are compared with each other and a quantitative agreement is found. However, the simulation analysis appears to be more promising since, in contrast to the integral equation theory in which the spinodal lines can only be approached, information on the microscopic structure of the new phases can be obtained.

PACS number(s): 61.20.Gy, 61.20.Ja, 64.60.-i

I. INTRODUCTION

It is well known that the stability of thermodynamic equilibrium states is expressed by the conditions

$$c_V \geq 0, \qquad K_T \geq 0, \quad \text{and} \quad \left(\frac{\partial^2 G}{\partial N^2}\right)_{P,T} \geq 0 \quad , \tag{1}$$

which identify, respectively, the thermal, the mechanical and the chemical stabilities. Here, c_V is the heat capacity at constant volume, K_T the isothermal compressibility, G the Gibbs free energy and N the number of particles. The locus of points in which the stability conditions are violated defines the spinodal lines of the system, whereas the regions of the state diagram delimited by these lines represent two-phases equilibrium states.

In a binary mixture, the loss of the mechanical stability indicates the onset of an equilibrium between a condensed and an evaporated phase, or a condensation/evaporation (C/E) transition. Correspondingly, the loss of the chemical stability indicates the onset of an equilibrium between two phases with different compositions, or a mixing/demixing (M/D) transition. However, in real situations, one usually gets transitions of a combined type.

Until recently, the phase transitions of binary fluids were described by integral equation theories in which the spinodal lines were determined by finding divergences either in the isothermal compressibility or in the macroscopic composition-composition fluctuations. Along these lines the group of Messina studied both mixtures of Lennard-Jones [1–3] and of hard sphere attractive Yukawa particles [4,5], Biben and Hansen [6] binary mixtures of large and small hard spheres and Belloni [7] binary mixtures of asymmetrical polyelectrolytes.

Although in some cases there was a satisfactory agreement with simulation data [4] and also with experimental data on sterically stabilized silica particles [8], all these approaches were not pushed to the level of quantitatively predict the kind of transition mechanism, once a given path in the parameter phase space was chosen. This goal has been achieved by the work of Parola and Reatto [9,10] and by that of Forstmann and coworkers [11,12].

In this paper, together with a review of the theoretical approach of Chen and Forstmann [11], we present a study of binary Lennard-Jones mixtures. The theoretical predictions, coming from the solution of the HMSA equations, are contrasted and compared with data obtained from Parallel Molecular Dynamics (PMD) simulations.

As far as the theory is concerned, the spinodal lines are located by finding the zero of the smallest eigenvalue associated with the diagonalization of an expansion of the grand free energy of the system, while the transition mechanism is determined from the associated eigenvector, which

gives indications about the most unstable linear combination of fluctuations. From the point of view of the simulation, the transitions are identified and located by recording the potential energy of interaction of the two species U_{12} (the so-called "interfacial" energy), and the "global" and "type" entropies, the last quantities being related to the spread-out of particles through the simulation box. We note that, since such quantities can only be efficiently computed for very large systems [13,14], we are forced to use PMD.

After a brief discussion of the statistical mechanics description of the instabilities (Sect. II) we present, in Sect. III, both the integral equation and the simulation methods. Section IV is devoted to the presentation of the results. A phase diagram in the $\epsilon_{12} - T$ plane (respectively the cross interaction strength and the temperature) is determined, and a discussion of the different regions is given. Conclusions and comments are also given in this last Section.

II. STATISTICAL MECHANICS OF CHEMICAL AND MECHANICAL INSTABILITIES

Since the work of Bhatia and Thornton [15], it is known that the isothermal compressibility and the density derivative of the Gibbs free energy are linked to the long wavelength limits of the total number density fluctuations

$$\delta n^{\mathrm{N}}(r) = \delta n_1(r) + \delta n_2(r) \quad , \tag{2}$$

and of the composition fluctuations

$$\delta n^{\mathrm{C}}(r) = (1 - x_1)\delta n_1(r) - x_1 \delta n_2(r) \quad , \tag{3}$$

where the sub-indices refer to the two species, $x_1 = N_1/N$ is the number fraction of species 1 and $\delta n_1(r) = n_1(r) - \overline{n_1}$ is the number fluctuation of species 1, with $\overline{n_1}$ its homogeneous density.

The relations derived by Bhatia and Thornton are

$$S_{\mathrm{NN}}(k) = \frac{1}{N}\langle \delta n_k^{\mathrm{N}} \delta n_{-k}^{\mathrm{N}} \rangle \quad \stackrel{k=0}{\longrightarrow} \quad n k_B T K_T + \Delta^2 N k_B T \Big/ \left(\frac{\partial^2 G}{\partial x_1^2} \right)_{T,P,N} \tag{4}$$

$$S_{\mathrm{NC}}(k) = \frac{1}{N}\langle \delta n_k^{\mathrm{N}} \delta n_{-k}^{\mathrm{C}} \rangle \quad \stackrel{k=0}{\longrightarrow} \quad -x_1 x_2 \Delta N k_B T \Big/ \left(\frac{\partial^2 G}{\partial x_1^2} \right)_{T,P,N} \tag{5}$$

$$S_{\mathrm{CC}}(k) = \frac{1}{N}\langle \delta n_k^{\mathrm{C}} \delta n_{-k}^{\mathrm{C}} \rangle \quad \stackrel{k=0}{\longrightarrow} \quad (x_1 x_2)^{1/2} N k_B T \Big/ \left(\frac{\partial^2 G}{\partial x_1^2} \right)_{T,P,N} \quad , \tag{6}$$

in which the $\delta n_k^{\mathrm{N,C}}$ are the Fourier components of the fluctuations and Δ is the dilatation factor defined by $\Delta = n(v_1 - v_2)$, with v_1 and v_2 the partial molar volumes of the two species. By remembering eq. (1), the spinodal lines are identified by divergences in the $k = 0$ limit of the Bhatia-Thornton structure factors or, more physically, by singularities in the total concentration and composition fluctuations.

It is only recently that these equations have been inserted in statistical mechanics schemes, which allow the clear identification of the transition mechanism (M/D, C/E and any combination of the two), and the quantitative location of the spinodal lines [9,11,16]. Here, we give the main steps of the approach developed by Chen and Forstmann [11,12].

This approach starts from the functional expansion of the grand free energy of the system, $\Omega(T, V, \mu_\alpha; [n_\alpha])$, around the equilibrium densities n_α ($\alpha = 1, 2$), as it is given by the density functional theory [17]. By truncating the expansion at the second order we have:

$$\delta\Omega \approx \frac{1}{2} \int\int \sum_\alpha \sum_\beta \left. \frac{\delta^2 \Omega}{\delta n_\alpha(\vec{r}_1) \delta n_\beta(\vec{r}_2)} \right|_{eq} \delta n_\alpha(\vec{r}_1) \delta n_\beta(\vec{r}_2) d\vec{r}_1 d\vec{r}_2 \quad , \tag{7}$$

where the functional derivatives of Ω are related to the direct correlation functions $c_{\alpha\beta}(\vec{r}_1, \vec{r}_2)$ through:

$$\left. \frac{\delta^2 \Omega}{\delta n_\alpha(\vec{r}_1) \delta n_\beta(\vec{r}_2)} \right|_{eq} = k_B T \left[\frac{\delta_{\alpha\beta} \delta(\vec{r}_1 - \vec{r}_2)}{n_\alpha} - c_{\alpha\beta}(\vec{r}_1, \vec{r}_2) \right] \quad , \tag{8}$$

By introducing the total correlation functions $h_{\alpha\beta}(r)$, via the Ornstein-Zernike equations, and the total density and composition fluctuations of eqs. (2) and (3), the Fourier transform of eq. (7) can be rewritten as a function of the fluctuations themselves and of a correlation matrix, $\mathbf{M}(k)$,

whose elements are linked to the Bhatia-Thornton structure factors. By diagonalizing such a matrix, the following expression is obtained:

$$\delta\Omega(\mathbf{M}(k)) = \frac{k_B T}{2V} \sum_k [\lambda_1(k)|\delta\overline{n}_1(k)|^2 + \lambda_2(k)|\delta\overline{n}_2(k)|^2] \quad , \tag{9}$$

in which the fluctuation terms $\delta\overline{n}_{1,2}(k)$ only appear to the square. They are defined by

$$\delta\overline{n}_i(k) = X_{i,1}(k) n^{-1/2} \delta n^{\mathrm{N}}(k) + X_{i,2}(k)(n/x_1x_2)^{1/2} \delta n^{\mathrm{C}}(k) \quad , \tag{10}$$

where the vector $\vec{X}_i(k)$ is the eigenvector of the diagonalization whose eigenvalues, $\lambda_{1,2}(k)$, are

$$\lambda_{1,2}(k) = \left(M_{\mathrm{NN}}(k) + M_{\mathrm{CC}}(k) \mp \sqrt{(M_{\mathrm{NN}}(k) - M_{\mathrm{CC}}(k))^2 + 4M_{\mathrm{NC}}(k)} \right)/2 \quad . \tag{11}$$

The Bhatia-Thornton structure factors are linked to the elements of the matrix $\mathbf{M}(k)$ by

$$S_{\mathrm{NN}}(k) = \mathbf{M}^{-1}_{\mathrm{NN}} \tag{12}$$

$$S_{\mathrm{NC}}(k) = x_1x_2\mathbf{M}^{-1}_{\mathrm{NC}} \tag{13}$$

$$S_{\mathrm{CC}}(k) = (x_1x_2)^{1/2}\mathbf{M}^{-1}_{\mathrm{CC}} \quad . \tag{14}$$

In summary, equation (9), plus eqs. (10) $\div$ (14) and eqs. (4 $\div$ 6), tells us the following:

- a stable homogeneous phase has all eigenvalues larger than zero;
- as the stability border is approached, some fluctuations start to diverge;
- the spinodal line is signalled by one eigenvalue going to zero;
- the related eigenvector defines the combination of fluctuations which are unstable at the spinodal line;
- such a combination tells to which extent the transition is C/E and/or a M/D phase transition.

These points can be quantitatively analysed by providing a theory to evaluate the Bhatia-Thornton structure factors and by making the assumption that the instabilities are originated only at $k = 0$. The theory to evaluate structural functions is discussed in the first part of the next section.

III. METHODS TO RECONSTRUCT THE STATE DIAGRAM

To localize the spinodal lines, to characterize the transition mechanism and to make a cross check of the results and observations, we used both integral equation theory and parallel molecular dynamics simulations.

A. Integral Equation approach

The needed structural functions are obtained by solving the Ornstein-Zernike equations

$$h_{\alpha\beta}(r) = c_{\alpha\beta}(r) + n \sum_\lambda x_\lambda \int h_{\alpha\lambda}(r) c_{\lambda\beta}(|\vec{r} - \vec{r}'|) d\vec{r}' \quad , \tag{15}$$

together with "closure" equations. In view of the coming applications, we chose the HMSA closure [18]:

$$h_{\alpha\beta}(r) = -1 + \exp[-\beta v^{\mathrm{rep}}_{\alpha\beta}(r)] \left(1 + \frac{\exp\big(f(r)[h_{\alpha\beta}(r) - c_{\alpha\beta}(r) - \beta v^{\mathrm{att}}_{\alpha\beta}(r)]\big) - 1}{f(r)} \right) \quad , \tag{16}$$

where the mixing function $f(r) = 1 - \exp(-\xi r)$ contains a parameter ξ which is fixed by the requirement of thermodynamic consistency

$$4\pi n \int_0^\infty dr \quad r^2 \sum_{\alpha\beta} x_\alpha x_\beta c_{\alpha\beta}(r) = \frac{\partial}{\partial n}\left[\frac{2\pi n^2 \beta}{3}\int_0^\infty dr \quad r^3 \sum_{\alpha\beta} x_\alpha x_\beta \frac{dv_{\alpha\beta}(r)}{dr} g_{\alpha\beta}(r)\right] \quad . \tag{17}$$

The purely repulsive, $v_{\alpha\beta}^{\rm rep}(r)$, and attractive, $v_{\alpha\beta}^{\rm att}(r)$, part of the particle-particle interaction potential are obtained according to the Weeks *et al.* [19] procedure.

Once the previous set of equations is solved, the structure factors are obtained from the Fourier transform of the three correlation functions $h_{\alpha\beta}(r) = g_{\alpha\beta}(r) - 1$

$$S_{\rm NN}(k) = 1 + n[x_1^2 \tilde{h}_{11}(k) + x_2^2 \tilde{h}_{22}(k) + 2x_1 x_2 \tilde{h}_{12}(k)] \tag{18}$$

$$S_{\rm NC}(k) = n x_1 x_2 [x_1 \tilde{h}_{11}(k) - x_2 \tilde{h}_{22}(k) + (x_2 - x_1)\tilde{h}_{12}(k)] \tag{19}$$

$$S_{\rm CC}(k) = 1 + n x_1 x_2 [\tilde{h}_{11}(k) + \tilde{h}_{22}(k) - 2\tilde{h}_{12}(k)] \quad . \tag{20}$$

All the other quantities needed for the spinodal lines, and listed in the previous section, are determined in a straightforward way.

However, by using integral equation schemes, the spinodal lines can only be "approached" from the stable homogeneous single phase region, and the location of them is only possible by extrapolation. This is due to the breakdown of the involved numerical procedure which, in turn, is induced by the coming singularities in the correlation functions. As a consequence, no information is obtained on the microscopic structure of the new phases which appear once the spinodal lines are crossed. Such kind of question can only be addressed by performing computer simulations.

B. Parallel Molecular Dynamics approach

The Parallel Molecular Dynamics (PMD) simulation approach has been adopted in order to have as many particles as possible in the same run.

The algorithm adopted exploits the short-range nature of the chosen potential (12-6 Lennard-Jones shifted at the cutoff radius $r_{\rm cut}$). A Verlet neighbour list is built in order to calculate the forces acting on the particles. The list is updated only when a particle has moved beyond a "safe" shell $r_{\rm safe} > r_{\rm cut}$. The "velocity Verlet" time integration scheme has been adopted [20].

The parallelization is based on the "replicated data" strategy [21]. The particles are evenly distributed among the processors, with no reference to their spatial position. The Verlet neighbour list is also distributed among the processors. When the list is built and when the particle status is updated, a systolic loop is used to pass the data among the processors. Clearly this entails a large amount of communications (all-to-all broadcast). We made our runs on an IBM SP1 with 32 processors (a small/medium size parallel machine). More sophisticated schemes would be possible (and necessary) with a larger machine (and a larger number of particles), exploiting a spatial decomposition and, therefore, only communications between neigbour coarse-grained cells.

Apart from the standard quantities needed for the system equilibration in the one-phase region (kinetic, potential and total energies, order parameters), we also monitored two different kind of quantities:
the interfacial energy

$$U_{\rm interf} \equiv U_{12} = \sum_{i=1}^{N_1}\sum_{j=1}^{N_2} v_{12}(r_{ij}) \quad , \tag{21}$$

and the entropy

$$S = -\frac{1}{\ln N_\mu}\sum_{i=1}^{N_\mu} \frac{n_i}{N} \ln \frac{n_i}{N} \quad , \tag{22}$$

where N_μ is the number of coarse-grained cells and n_i is the number of particle in the i-th cell.

It is expected that these quantities, for very large systems, are sensitive to phase separation processes. Whenever the two different kinds of particles try to demix (with formation of "interfaces"), the absolute value of $U_{\rm interf}$ reduces drastically. To its actual value will only contribute particles in the interfacial regions, with a reduction in the number of terms in the double summmation of eq. (21). If there is a separation in a dense and evaporated phase with no demixing, the many particles in the dense phase will experience a shorter average distance with a global increase of the absolute value of $U_{\rm interf}$.

The entropy, being a measure of how the particles distribute in the simulation box, is also a good indicator for the transition, and it can be calculated disregarding the type ("global") or for each type of particle ("type"). We normalize S with respect to the ideal case ($T = \infty$) of a uniform random distribution, $S^* = S/S_{\rm ideal}$, with

$$S_{\rm ideal} \simeq -\frac{1}{\ln N_\mu} \sum_{i=1}^{N_\mu} \sum_{n_i} p(n_i) \frac{n_i}{N} \ln \frac{n_i}{N} \quad , \tag{23}$$

where we used the Poisson distribution

$$p(n_i) = \left(\frac{N}{N_\mu}\right)^{n_i} \frac{\exp(-N/N_\mu)}{n_i!} \quad . \tag{24}$$

In the high temperature one-phase region, both values of $S^*_{\rm global}$ and $S^*_{\rm type}$ approach 1, whereas in the two-phase region they will have smaller and equal values (C/E transition) or smaller and different values (M/D transition).

IV. RESULTS AND CONCLUSIONS

We investigated binary mixtures of particles interacting with a Lennard-Jones 12-6 potential

$$v_{\alpha\beta}(r) = 4\epsilon_{\alpha\beta} \left[\left(\frac{\sigma_{\alpha\beta}}{r}\right)^{12} - \left(\frac{\sigma_{\alpha\beta}}{r}\right)^{6} \right] \quad . \tag{25}$$

We focused on mixtures characterized, at a microscopic level, by equal diameters $\sigma_{11} = \sigma_{12} = \sigma_{22}$ (under the rule $\sigma_{\alpha\beta} = (\sigma_\alpha + \sigma_\beta)/2$) and by interaction strength parameters $\epsilon_{11} = \epsilon_{22} \neq \epsilon_{12}$. On a macroscopic level they are characterized by number fractions $x_1 = x_2 = 0.5$, by a total number density $n = 0.5\sigma_1^3$ and by a temperature T. Such mixtures are called "symmetrical" since particles 1 and 2 play the same role. We used them to test the internal correctness and stability of the used approaches and, in particular, of the PMD simulations. The case of asymmetrical mixtures will be the subject of a forthcoming publication. In the following calculations, all quantities are expressed in reduced units (lengths rescaled by σ_1 and energies by ϵ_{11}).

From the theoretical point of view, and as contrasted to real binary mixtures [22], symmetrical mixtures show well characterized behaviour since the correlation matrix $\mathbf{M}(k)$ is already diagonal, with eigenvalues

$$\lambda_{\rm N}(k) = M_{\rm NN}(k) = S^{-1}_{\rm NN}(k) \tag{26}$$

$$\lambda_{\rm C}(k) = M_{\rm CC}(k) = x_1 x_2 S^{-1}_{\rm CC}(k) \quad , \tag{27}$$

and since the difference in the partial volumes, Δ, is identically zero. These characteristics indicate that the transition mechanism of symmetric mixtures is either a "pure" C/E or a "pure" M/D mechanism.

The simulation data are obtained by studying systems with $N = 16384$ L-J particles. The time step chosen (in reduced units) is $\Delta t^* = 0.01$. Block averages are taken after an equilibration period which depends on the temperature and on the previous history (usually ≈ 30000 time steps). The equilibration is obtained by re-shuffling the particle velocities every $50 \div 100$ time steps, according to a Maxwellian distribution [23]. The cutoff distance of the interaction potential is $r^*_{\rm cut} = 4.0$. By using these parameters and by updating the Verlet neighbour list for a safe-shell diameter $r^*_{\rm safe} = 6.0$ (i.e. ≈ 20 time steps), typical CPU times on the IBM SP1 (4 nodes) are $12 \div 20$ s/step. Finally, we have chosen $N_\mu = 512$ coarse-grained cells for the entropy evaluation.

Results from the HMSA scheme are obtained by using a variable number of points in the FFT (up to 16384). We found that, in approaching the spinodal line, the stability of the numerical solution method (we used the Ng iteration procedure [24]) improves as the real-space interval, on which the method works, is enlarged.

To study the M/D and the C/E transitions we chose 5 different systems, each one with a given value of ϵ_{12}.

The HMSA results for the $k = 0$ eigenvalues of the matrix $\mathbf{M}(k)$ are given in Fig.1 as a function of the temperature. For small value of ϵ_{12} ($\epsilon_{12} = 0.4, 0.6$), the $\lambda_{\rm C}$ eigenvalue approaches zero ($S_{\rm CC}(0) \to \infty$) as the temperature is reduced. Microscopically this corresponds to a divergence in the homogeneous composition fluctuations and to an approach to a pure M/D transition (see also eq. (20)). As ϵ_{12} is increased ($\epsilon_{12} = 0.75, 1.2$), particles of species 1 "like" more particles of

species 2 and, by decreasing T, the λ_N eigenvalue goes to zero ($S_{NN} \to \infty$): the systems approach a pure C/E transition. For $\epsilon_{12} = 0.7$ a competition between the two different kinds of mechanisms is found.

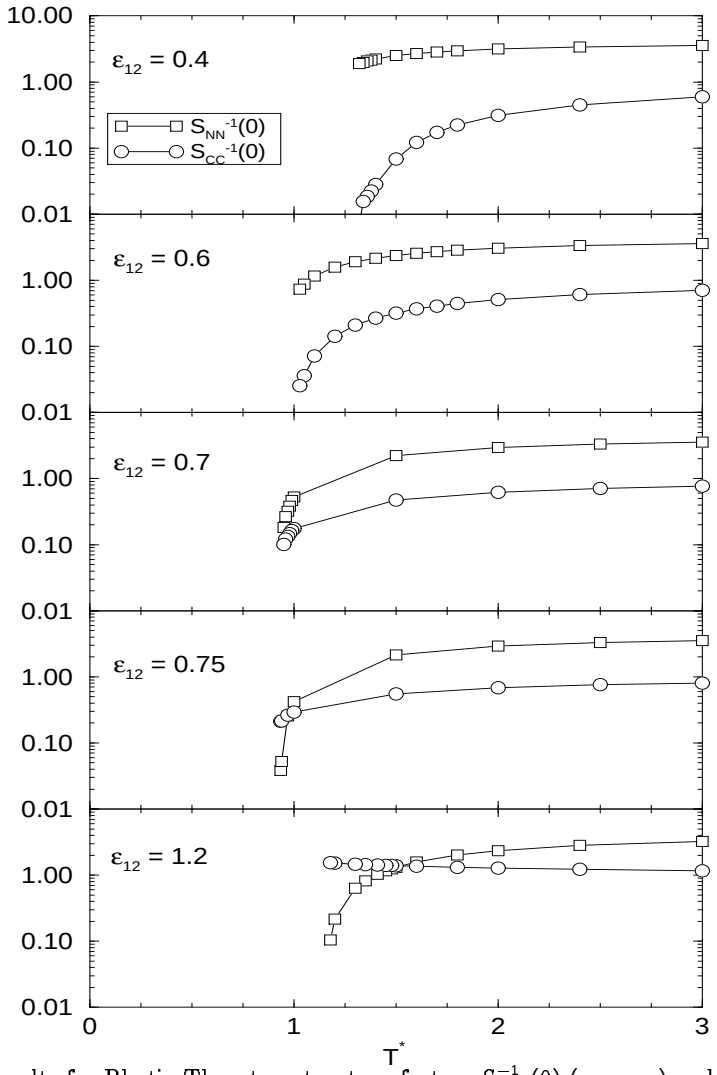

FIG. 1. HMSA results for Bhatia-Thornton structure factors $S_{NN}^{-1}(0)$ (squares) and $S_{CC}^{-1}(0)$ (circles) vs T^*, for different values of ϵ_{12} (0.4, 0.6, 0.7, 0.75 and 1.2). Other system parameters are listed in the text.

The same 5 different systems are also studied by PMD. Fig.2 shows the simulation data for $U_{\rm interf}$ and for S^* for the system at $\epsilon_{12} = 0.4$. At $T = 1.4$ the energy line has a drastic change of slope, while, almost at the same temperature, $S^*_{\rm global}$ and $S^*_{\rm type}$ start to be quantitatively different. After the bending point $U_{\rm interf}$ goes toward zero meaning that the number of interacting pairs 1-2 is reduced and that, essentially, the particles are demixed. At the same time, the separation of the two kinds of entropies indicates that i) globally (no distinction between particles), the system is still spread-out uniformly among the coarse-grained cells (small decrease of $S^*_{\rm global}$) and that ii) particles of one species are grouped in a smaller number of such cells (larger decrease of ${}^*S_{\rm type}$). These last results, together with the inspection of configuration snapshots, are consistent with the M/D picture resulting from $U_{\rm interf}$ and from HMSA.

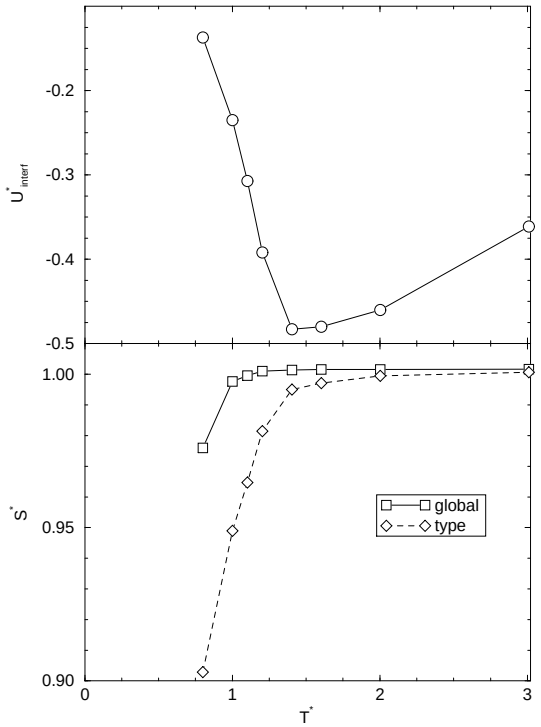

FIG. 2. MD simulation results for U^*_{interf} and S^* (both "global" and "type") vs T^*, for $\epsilon_{12} = 0.4$.

Fig.3 shows the same quantities but for $\epsilon_{12} = 1.2$. In this case, after the bending, the energy decreases and the two entropies follow each other. It is easily understood that these behaviour support a microscopic picture corresponding to a C/E mechanism, in agreement with the HMSA results.

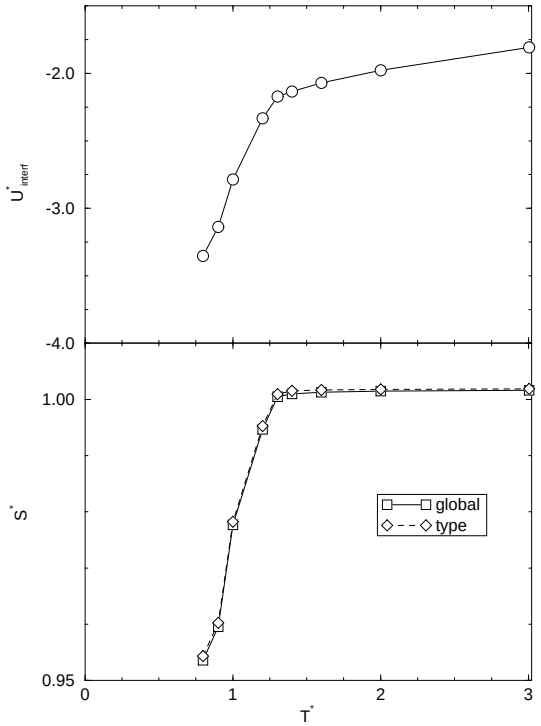

FIG. 3. Same as **Fig.2** but for $\epsilon_{12} = 1.2$.

In Fig.4 all results are summarized and the spinodal line in the plane (ϵ_{12}, T) is localized. In the case of PMD, error bars connect the closest temperatures studied between which the transition is taking place. The agreement between HMSA and PMD data is quantitative. For $\epsilon_{12} < 0.7$, the system makes a M/D transition while for $\epsilon_{12} > 0.7$ it makes a C/E transition.

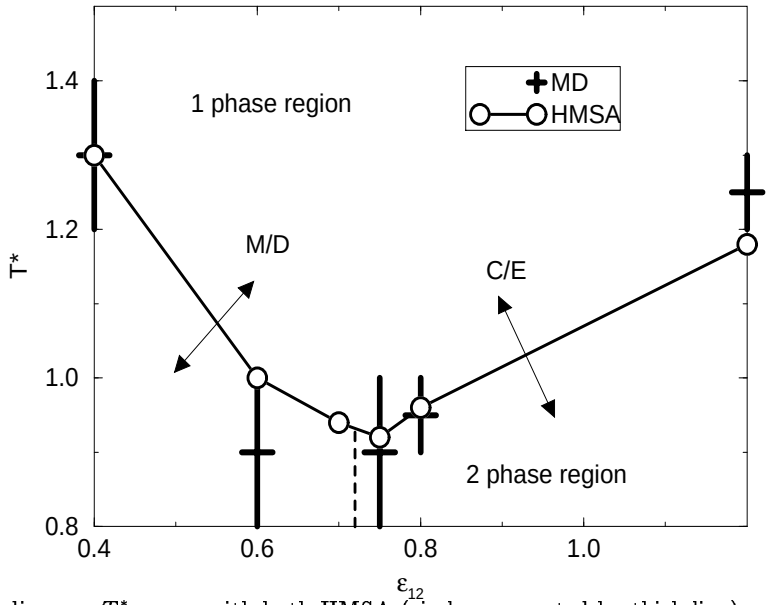

FIG. 4. Phase diagram T^* vs ϵ_{12} with both HMSA (circles connected by thick line) and MD simulation results (thick error bars); the nature of the transition between 1-phase region and 2-phase regions (C/E or M/D) is also indicated.

In the last figure (Fig.5) we present the pair distribution functions $g_{11}(r), g_{12}(r)$ for temperature above and below the transition and for $\epsilon_{12} = 0.4, 1.2$. In Fig.5.a ($\epsilon_{12} = 0.4$) we observe that $g_{11}(r)$ develops a lot of structure as the temperature is reduced, while the opposite is true for $g_{12}(r)$. More interesting is the decay of such functions. They reach the value of 1 for $r* \approx 15$, and such a distance can be interpreted as a measure of the size of the clusters of the new phases [13]. Since the value of $r*$ is almost half of the simulation box size, it also indicates that the systems are at equilibrium, and that in the simulation box we have only two regions (clusters) which correspond to the new phases. For $\epsilon_{12} = 1.2$ (Fig.5.b) both $g_{11}(r)$ and $g_{12}(r)$ continue to be very structured, even below the transition temperature.

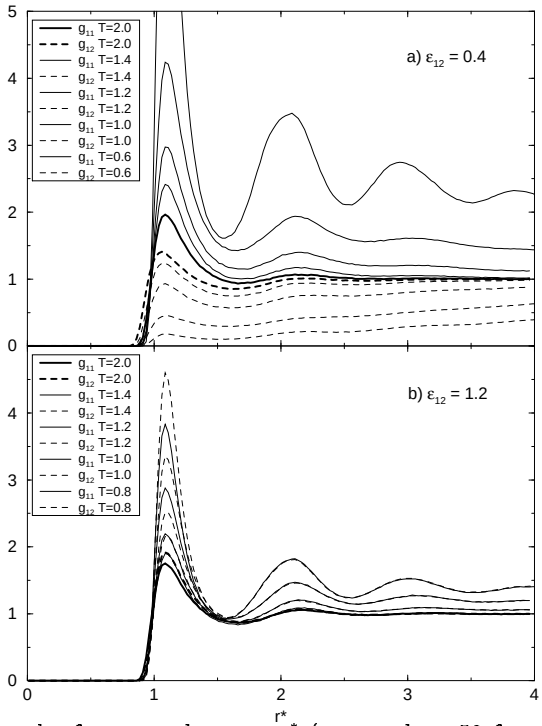

FIG. 5. MD simulation results for g_{11} and g_{12} vs r^* (averaged on 50 frames), for two different values of ϵ_{12} (**a** 0.4 and **b** 1.2) and five different values of T^*. In both cases, thickest lines indicate the highest temperature $T^* = 2.0$.

Although these findings are once more consistent with previous consideration, *i.e.* M/D transi-

tion for $\epsilon_{12} = 0.4$ and C/E transition for $\epsilon_{12} = 1.2$, we note that no direct information is obtained on the microscopic structure of the new phases. This analysis can only be performed by first choosing a criteria to label particles belonging to each phase (possibly by using a Voronoi tessellation of the simulation box), and then by performing structural and quantitative analysis on these sets of particles. We also remember that information on the new phases and, this time, on the binodal lines can be obtained by using the Gibbs Monte Carlo method [25]. Studies along these lines, together with the extension to asymmetrical systems and to noble gas binary mixtures at high pressure, are in progress.

ACKNOWLEDGEMENTS

This work has been carried out with the financial support of the "Regione Autonoma della Sardegna". Fruitful discussions with M. Rovere and E. Bonomi as well as help in the setup of the PMD code by M. Valentini, P. Rossi and A. Scheinine are acknowledged.

REFERENCES

[1] G. Malescio, *Phys. Rev* **A 42**, 2211 (1990).

[2] G. Malescio, *Phys. Rev* **A 42**, 6241 (1990).

[3] Maria C. Abramo and C. Caccamo, *Phys. Lett* **A 166**, 70 (1992).

[4] C. Caccamo, G. Giunta, and C. Hoheisel, *Phys. Lett.* **A 158**, 325 (1991).

[5] C. Caccamo and G. Giunta, *Mol. Phys.* **78**, 83 (1993).

[6] T. Biben and J.P. Hansen, *Phys. Rev. Lett.* **66**, 2215 (1991).

[7] L. Belloni, *Phys. Rev. Lett.* **57**, 2026 (1986).

[8] J.S. van Duijneveldt, A.W. Heinen, and H.N.W. Lekkerkerker, *Europhys. Lett.* **21**, 369 (1993).

[9] A. Parola and L. Reatto, *Phys. Rev.* **A 44**, 6600 (1991).

[10] A. Parola and L. Reatto, *J. Phys.: Condens. Matter* **5**, B165 (1992).

[11] X.S. Chen and F. Forstmann, *J. Chem. Phys.* **97**, 3696 (1992).

[12] X.S. Chen and F. Forstmann, *Mol. Phys.* **76**, 1203 (1992).

[13] S.W. Koch, R.C. Desai, and F.F. Abraham, *Phys. Rev.* **A 27**, 2152 (1983).

[14] W.J. Ma, A. Maritan, J.R. Banavar, and J. Koplik, *Phys. Rev.* **A 45**, R5347 (1992).

[15] A.B. Bhatia and D.E. Thornton, *Phys. Rev.* **B2**, 3004 (1970).

[16] Similarities and differences between these two approaches will be a subject of a coming publication.

[17] R. Evans, *Adv Phys.* **28**, 143 (1979).

[18] G. Zerah and J.P. Hansen, *J. Chem. Phys.* **84**, 2336 (1986).

[19] J.D. Weeks, D Chandler, and H.C. Andersen, *J. Chem. Phys.* **54**, 5237 (1971).

[20] M.P. Allen and D.J. Tildesley, *Computer Simulation of Liquids*, Oxford Univ. Press, New York (1987).

[21] W. Smith and T.R. Forester, *Computer Physics Communication* **79**, 52 (1994).

[22] A. Deerenberg, J.A. Schouten, and N.J. Trappeniers, *Physica* **A 101**, 459 (1980).

[23] E. Bonomi, *J. Stat. Phys.* **39**, 167 (1985).

[24] J.C. Ng, *J. Chem. Phys.* **61**, 2680 (1974).

[25] A.Z. Panagiotopoulos, N. Quirke, M. Stapleton, and D.J. Tildesley, *Mol. Phys.* **63**, 527 (1988).